PCCP
Physical Chemistry Chemical Physics

Accepted Manuscript

This article can be cited before page numbers have been issued, to do this please use: X. Deraet, E. Desmedt, R. Van Lommel, V. Van Speybroeck and F. De Proft, *Phys. Chem. Chem. Phys.*, 2023, DOI: 10.1039/D3CP03137C.

ROYAL SOCIETY OF CHEMISTRY

rsc.li/pccp

The Electrophilic Aromatic Bromination of Benzenes: Mechanistic and Regioselective Insights from Density Functional Theory

Xavier Deraet,[a] Eline Desmedt,[a] Ruben Van Lommel,[a,b] Veronique Van Speybroeck,[c] Frank De Proft*[a]

[a] Department of General Chemistry (ALGC), Vrije Universiteit Brussel (VUB), Pleinlaan 2, 1050 Elsene, Brussels, Belgium

[b] Molecular Design and Synthesis, Department of Chemistry, KU Leuven, Celestijnenlaan 200F Leuven Chem&Tech, box 2404, 3001 Leuven, Belgium

[c] Center of Molecular Modeling, Ghent University, Technologiepark 46, 9052 Zwijnaarde, Belgium

Corresponding author: Prof. Frank De Proft (fdeprof@vub.be)

Abstract

The HBr-assisted electrophilic aromatic bromination of benzene, anisole and nitrobenzene was investigated using static DFT calculations in gas phase and implicit apolar (CCl4) and polar (acetonitrile) solvent models at the ωB97X-D/cc-pVTZ level of theory. The reaction profiles corresponding to either a direct substitution reaction or an addition-elimination process were constructed and insight into the preferred regioselectivity was provided using a combination of conceptual DFT reactivity indices, aromaticity indices, Wiberg bond indices and the non-covalent interaction index. Our results show that under the considered reaction conditions the bromination reaction preferentially occurs through an addition-elimination mechanism and without formation of a stable charged Wheland intermediate. The *ortho*/*para* directing effect of the electron-donating methoxy-group in anisole was ascribed to a synergy between strong electron delocalisation and attractive interactions. In contrast, the preferred *meta*-addition on nitrobenzene could not be traced back to any of these effects, nor to the intrinsic reactivity property of the reactant. In this case, an electrostatic clash between the *ipso*-carbon of the ring and the nitrogen atom resulting from the later nature of the rate-determining step, with respect to anisole, appeared to play a crucial role.

Introduction

Aromatic substitutions are one of the most common organic transformations found in both the academia and pharmaceutical industry.[1] The conjugated aryls allow nucleophilic and electrophilic species to attach on the ring in the so-called nucleophilic (S_NAr) or electrophilic aromatic substitution (S_EAr), respectively.[2] First reports of these reactions date back over 150 years, they have been reviewed extensively since the 60's[3-6] and have consequently made their entry in the standard undergraduate organic chemistry course.[7,8] Thus, it might come as a surprise that these century-old reactions are still today a focus of both experimental and theoretical research. An explanation for this can be found in its mechanism. Indeed, in the last decade, both experimental and theoretical studies have appeared that question the traditional mechanism, which proceeds in a stepwise fashion through the formation of an ionic intermediate (Meisenheimer complex (S_NAr) and Wheland intermediate (S_EAr), Figure 1a). Instead, alternative (concerted) mechanisms have been postulated when the ionic intermediate would otherwise be insufficiently stable.[9-14] These studies have

reinvigorated the interest towards aromatic substitutions and inspired several groups to investigate the factors that influence its mode of action.[15-19]

Among all applicable electrophiles for the S_EAr transformation, the halogenation of benzene through Cl_2 or Br_2 is the most elementary system. Although significant efforts are still being made to develop more effective and greener catalysts for the electrophilic halogenation of arene rings, some groups have also reported the non-catalysed aromatic halogenation by using a high concentration of the halogen gas.[20-25] In this context, Galabov, Schaefer and Schleyer were the first to report a mechanism for the non-catalysed chlorination and bromination of simple aromatic rings.[26,27] These occur through either a concerted direct substitution or an addition-elimination mechanism and importantly do not involve the charged Wheland intermediate (Figure 1b). In a more recent combined experimental-computational study by the Genaev and Rzepa groups, the non-catalysed bromination of benzene was achieved by using high concentrations of Br_2 (5-14 M), resulting predominantly in bromobenzene.[26] The high concentration and observed kinetic order of Br_2 (4.80 ± 0.06) could be rationalized by a DFT-supported mechanism involving a cluster of 4 Br_2 molecules.

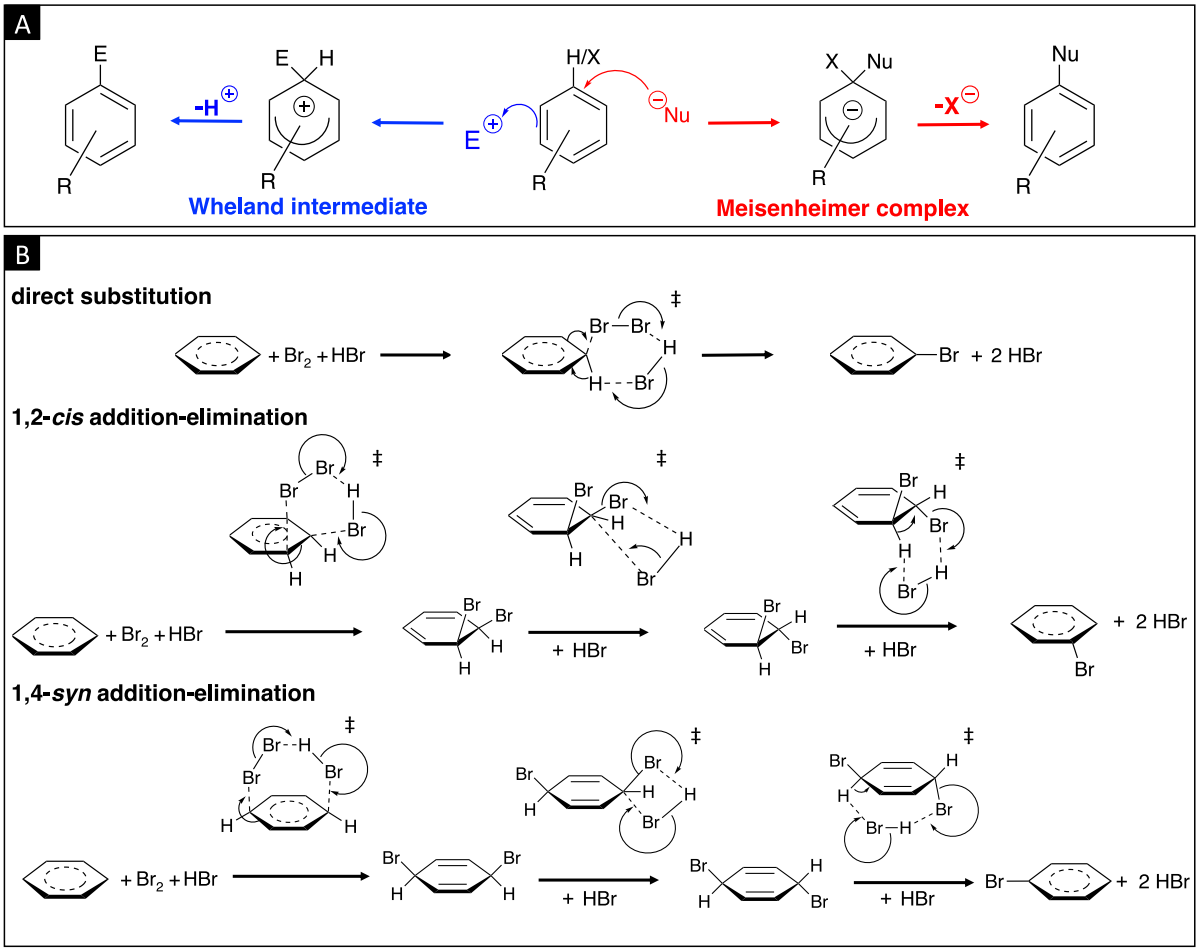

Figure 1. A) Classic two-step reaction mechanism for the electrophilic and nucleophilic aromatic substitution involving the formation of a Wheland or Meisenheimer complex, respectively. B) Overview of the alternative mechanisms for the electrophilic aromatic halogenation as mentioned in literature.[26,27]

Inspired by these findings, some of the authors of this work have previously investigated the effect of the solvent on the mechanism of the electrophilic chlorination of benzene.[16] A combination of *ab initio* metadynamics simulations and static DFT calculations revealed that a mechanistic cross-over can occur from an addition-elimination pathway to the classical

View Article Online
DOI: 10.1039/D3CP03137C

textbook mechanism. These cross-overs are induced by the extent of which the ionic Wheland intermediate and its counter-anion are stabilized through the electrostatic properties of the (a)polar solvent and potential explicit interactions. Furthermore, the occurrence and lifetime of this Wheland intermediate as well as the followed reaction mechanism is known to be heavily dependent on the molecular environment in which such an electrophilic aromatic substitution takes place. Hence, in a heterogeneous zeolitic environment the Wheland complex is often retrieved as a rather stable intermediate, whereas in a homogeneous medium this is much less the case.[29] In the present work, we extend this fundamental investigation towards the electrophilic aromatic bromination. In addition to assessing the effect of implicit solvent molecules on the mechanism, we will evaluate the (de-)activating effects and the regioselective control exerted by a substituent on the aryl ring, by considering both benzene, anisole and nitrobenzene as reactive species. Moreover, in accordance with the autocatalytic effect observed during the aromatic chlorination, the potential autocatalytic effect of HBr, which is generated during the reaction, will be taken into consideration. As such, this study aims to provide the field with an in-depth quantum chemical analysis of the mechanism of the non-catalysed bromination of arenes and in doing so contribute to the fundamental understanding of these chemical reactions.

Computational Methodology

All Density Functional Theory calculations were performed using the Gaussian quantum chemistry package (version G16.A.03).[30] In line with our previous study on the electrophilic aromatic chlorination,[16] all structures were optimised using the range-separated hybrid ωB97X-D functional[31] in combination with the cc-pVTZ basis set.[32] The nature of the stationary points was determined based on the number of negative eigenvalues of the Hessian matrix obtained from frequency calculations. The thermal correction to the Gibbs free energy was computed at room temperature (298.15 K) and pressure of 1 atm. Natural atomic charges[33] (NPA) and Wiberg bond indices[34] were determined using the NBO 3.1 program[35] as implemented in the Gaussian 16 package. The role of apolar (CCl_4) and polar (acetonitrile) solvent molecules on the energetics of the bromination reaction of benzene was implicitly taken into account by re-optimising the obtained geometries using the polarizable continuum SMD model[36] at the same level of theory. The coordinates of the optimised geometries can be found in the Supporting Information.

In order to assess whether intrinsic reactivity properties of anisole and nitrobenzene drive the regioselectivity of their electrophilic bromination reaction, both global and local conceptual DFT indices were determined within the finite difference approximation. The global softness (*S*), representing the propensity of the overall system to undergo charge transfer, was retrieved as the inverse of the difference between the vertical ionization potential (*I*) and electron affinity (*A*).[37] The condensed Fukui functions for electrophilic attack (f_k^-) were computed as the difference between the NPA atomic charges of the *N* and *N*-1 electron system and provided a local view on the regions that are the most prone to interact with the bromine electrophile.[38-40] The global softness and Fukui functions for electrophilic attack are expressed in equation 1 and 2, respectively:

$$S = \frac{1}{E(N-1) - 2E(N) - E(N+1)} = \frac{1}{I - A} \quad (1)$$

View Article Online
DOI: 10.1039/D3CP03137C

$$f_k^- = q_k^{N-1} - q_k^N \quad (2)$$

Since a temporary loss of aromaticity in the benzene ring is a key feature of the electrophilic aromatic substitution reaction, a series of geometrical (Harmonic Oscillator Model of Aromaticity[41] (HOMA), Bond Length Alternation[42] (BLA(1))) and electronic (Fluctuation index[43] (FLU), Bond Order Alternation[42] (BOA(1))) aromaticity indices for the rate-determining transition states was computed using the ESI-3D code.[44] Besides wavefunction files, this code requires the atomic overlap matrices of the structures of interest in order to define the electronic aromaticity indices. These matrices were constructed within the quantum theory of atoms in molecules using the AIMAll software.[45]

Next to fluctuations in aromaticity, the role of non-covalent interactions was also assessed using the Non-Covalent Interaction (NCI) index.[46] This index was computed with the NCIPLOT program[47] starting from the ωB97X-D/cc-pVTZ wavefunctions of the transition states of interest. This index is a semi-quantitative method that allows to differentiate between covalent and non-covalent interactions based on a plot of the reduced density gradient (s) versus the electron density. The reduced density gradient can be expressed as:

$$s = \frac{1}{2(3\pi^2)^{1/3}} \frac{|\nabla\rho|}{\rho^{4/3}} \quad (3)$$

This equation relies on the properties of the electron density, which displays a monotonic exponentially decreasing behaviour for increasing distances and reaches a cusp at the nuclear positions. Hence, regions far away from any nuclei will be described by low electron density values and large reduced density gradients. In contrast, since a covalent interaction can be associated to the common sharing of electrons, this type of interaction will be characterised by those regions of the s vs ρ plot for which the density is high and the reduced density gradient almost zero. Ultimately, the non-covalent interactions are determined by the presence of troughs at low density values (*i.e.* low density and reduced density gradient values) due to the annihilation of the reduced density gradient at these points.[46] The distinction between attractive and repulsive non-covalent interactions is determined by the sign of the second eigenvalue λ_2 of the electron-density Hessian matrix. Therefore, the reduced density gradient (s) is commonly plotted against the product of the electron density function (ρ) and the sign(λ_2). Attractive interactions, such as hydrogen bonding, are characterised by a negative value of λ_2, whereas a positive value of λ_2 corresponds to repulsive interactions, like steric clashes. The strength of these interactions can, in turn, be deduced from the density values of the low-gradient spikes. A three-dimensional representation of non-covalent interactions is obtained using the reduced gradient isosurfaces, which are generated for an isovalue of 0.5 with the VMD software.[48]

Results and Discussion

A view on the reaction mechanism of the bromination of benzene

In order to elucidate the role of the reaction medium, the polarity of the solvent and the presence of an acidic HBr molecule on the mechanistic aspects of the bromination of benzene, the Gibbs free energy profiles of three possible reaction pathways: *(i)* 1,2-*cis* addition-elimination, *(ii)* 1,4-*syn* addition-elimination and *(iii)* direct substitution, were investigated, as schematically indicated in Figure 1. The relative Gibbs free energies of the rate-determining

steps ($\Delta G^{\ddagger}$) computed at the ωB97X-D/cc-pVTZ level of theory are listed in Table 1, whereas the optimised geometries of all the considered structures in the various pathways are summarized in the Supporting Information. Throughout this paper, the Gibbs free energies are described with respect to the set of reactant molecules associated with the specific reaction. Moreover, given the kinetic control of the electrophilic aromatic bromination, the reaction barrier of the rate-determining reaction step was also computed using DLPNO-CCSD(T)[49,50] calculations with the ORCA software[51,52] on our ωB97X-D/cc-pVTZ geometries in gas phase. These activation energies can be found in the Supporting Information (Table S1) and are fully in line with the obtained DFT data, used in the upcoming discussion; the observed DLPNO-CCSD(T) trends in both regioselective and mechanistic preference are fully identical with those obtained at the ωB97X-D/cc-pVTZ level of theory.

The impact of the apolar dichloromethane (CCl_4) and polar acetonitrile (ACN) solvent on the Gibbs free reaction profiles was implicitly assessed by full re-optimisation of the various reaction species with the SMD solvation model.

Table 1. Relative Gibbs free energies ($\Delta G^{\ddagger}$, in kcal.mol^{-1}) and aromaticity indices for the rate-determining steps of the 1,4-*syn* addition-elimination (TS1), 1,2-*cis* addition-elimination (TS1*) and direct substitution (TS) of benzene determined at the ωB97X-D/cc-pVTZ level of theory.

Reaction medium	Cat.	Mechanism	$\Delta G^{\ddagger}$	HOMA[a]	BLA(1)[b]	BOA(1)[c]	FLU[d]
Gas	-	1,4-*syn* add-elim	63.7	0.900	0.027	0.136	0.007
Gas	-	1,2-*cis* add-elim	65.9	0.546	0.044	0.188	0.020
Gas	HBr	1,4-*syn* add-elim	53.3	0.579	0.047	0.221	0.021
Gas	HBr	1,2-*cis* add-elim	59.3	0.509	0.046	0.197	0.021
Gas	HBr	direct substitution	59.5	0.665	0.038	0.177	0.018
CCl_4	HBr	1,4-*syn* add-elim	49.7	0.511	0.049	0.223	0.023
CCl_4	HBr	1,2-*cis* add-elim	52.2	0.437	0.050	0.219	0.024
CCl_4	HBr	direct substitution	52.4	0.547	0.044	0.198	0.022
ACN	HBr	1,4-*syn* add-elim	36.0	0.369	0.053	0.236	0.027
ACN	HBr	1,2-*cis* add-elim	36.5	0.362	0.053	0.238	0.027
ACN	HBr	direct substitution	37.0	0.371	0.053	0.237	0.027

[a] Harmonic Oscillator Model of Aromaticity, [b] Bond Length Alternation, [c] Bond Order Alternation [d] Fluctuation index

The calculations in gas phase reveal that the bromination of benzene in the presence of a single Br_2 is not likely to occur through the classic electrophilic aromatic substitution mechanism as no Wheland intermediate could be found along the potential energy surface. In contrast, both the 1,2-*cis* and 1,4-*syn* addition-elimination reaction, which were already put forward by Galabov and Schleyer for both the bromination[26] and chlorination[27] of different benzenes, were fully characterized and the corresponding computed Gibbs free reaction profiles are shown in Figure 2. These profiles indicate an experimentally high to overcome activation energy for the rate-determining step, that is, leading to the transition state describing the addition of both bromine atoms to the ring system, of 63.7 kcal.mol^{-1} for the 1,4-*syn* pathway (TS1) and 65.9 kcal.mol^{-1} for the 1,2-*cis* addition elimination process (TS1*). These energetic barriers remain extremely high for both the *anti* (TS2) or *cis* (TS2*) isomerisation step as well as for the final elimination of HBr, yet the kinetic preference for the 1,4-*syn* addition-elimination reaction is retained throughout the entire reaction profile. It must nevertheless be stated that under experimental conditions the bromination of benzene always involves the use of a Lewis acid catalyst and therefore these high barriers should be

rationalized within the fundamental theoretical context of the proposed study. The preference for this pathway seems to be triggered by the extent by which the aromaticity of the six-membered benzene ring is affected during the actual addition of bromine. As can be observed from Table 1, the Harmonic Oscillator Model of Aromaticity[41] (HOMA) index reaches the value of 0.900 for the rate-determining transition state of the 1,4-*syn* pathway (TS1), while a serious decline towards 0.546 is obtained for the 1,2-*cis* pathway (TS1*). Since in this geometrical model, the aromatic benzene molecule is assigned a value of 1.00, it clearly turns out that the aromaticity in the former reaction mechanism is significantly less affected by the addition of Br_2. Alternatively, the aromatic fluctuation index (FLU), which relates to the electronic charge variation between neighbouring atoms in the cyclic systems,[43] seems to be larger for the 1,2-*cis* pathway (0.020) as compared to the 1,4-*syn* pathway (0.007), confirming the more pronounced aromatic character of the latter. As can be observed from Table 1, similar conclusions can also be drawn from other geometrical (Bond Length Alternation[42] (BLA(1))) and electronic (Bond Order Alternation[42] (BOA(1))) aromaticity indices for which holds that the lower the numerical value of the index, the more aromatic the considered system is. Hence, we conclude that the 1,2-*cis* addition-elimination pathway in gas phase is kinetically the least favourable due to a stronger reduction in aromaticity.

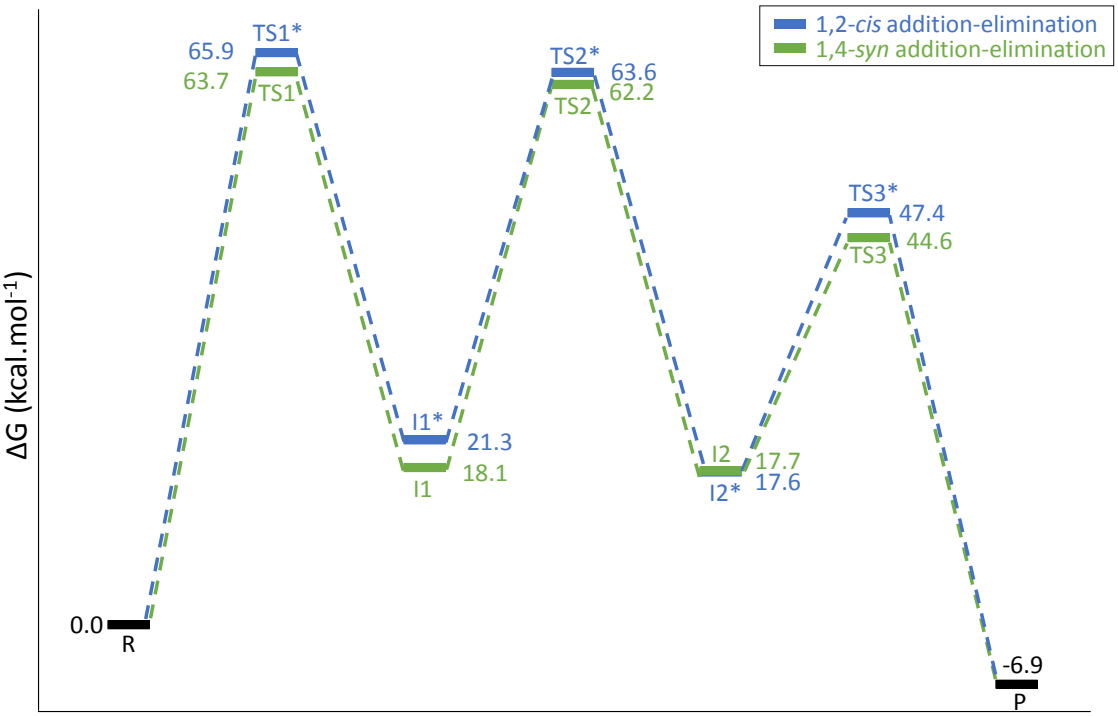

Figure 2. Gibbs free reaction profiles (in kcal.mol^{-1}) for the bromination of benzene in gas phase following the 1,2-*cis* (blue) or 1,4-*syn* (green) addition elimination pathway. The reactants (R) correspond to benzene and Br_2, while bromobenzene and HBr are obtained as products (P). These pathways consist of 3 consecutive transition states TS (addition, isomerisation and elimination) and 2 intermediate states I.

Given the high energetic requirements to overcome the initial step of both mechanisms, it is very unlikely that the bromination of benzene will take place under the considered conditions. However, in earlier work performed by some of the authors on the chlorination of benzene it was shown that the addition of an HCl molecule reduces the kinetic barrier of this reaction.[16] Based on these findings, we re-assessed the various reaction pathways for the bromination of benzene in the presence of a single HBr molecule (Figure 3). Inspired by the HCl-catalyzed chlorination, one could imagine HBr to actively participate in the first stages of the electrophilic bromination by transferring its proton to the Br_2 reagent, while its halogen is

incorporated onto the benzene ring. Ultimately, HBr is recovered at the end of the bromination process. As can be observed from Figure 3, the inclusion of HBr decreases the Gibbs free activation energy of the rate-determining transition state to 59.3 (-6.6) and 53.3 (-9.3) kcal.mol^{-1} for the 1,2-*cis* and 1,4-*syn* addition-elimination reaction, respectively. This confirms the beneficial influence of an inorganic acid on the kinetics of halogenation reactions on benzene, although this effect seems to be more pronounced for the chlorination, with a decrease of 9.8 (1,2-*cis*) and 19.8 (1,4-*syn*) kcal.mol^{-1},[16] than for the bromination. On the other hand, the introduction of this autocatalytic reagent does accentuate the preference for the 1,4-*syn* addition-elimination reaction, as the difference in activation energy between both processes increases to 5.9 kcal.mol^{-1}. In addition to these addition-elimination pathways, the presence of HBr also allows the bromination of benzene to occur through a direct substitution reaction mechanism, but still without formation of the classical Wheland intermediate. In this concerted mechanism, a single bromine atom originating from the Br_2 reagent is transferred to the benzene ring, whereas the dissociated HBr molecule accommodates the removal of the proton to restore aromaticity. The associated activation energy of this substitution (59.5 kcal.mol^{-1}) is found to be almost identical to that of the 1,2-*cis* addition-elimination and hence less favourable as compared to the 1,4-*syn* addition-elimination pathway.

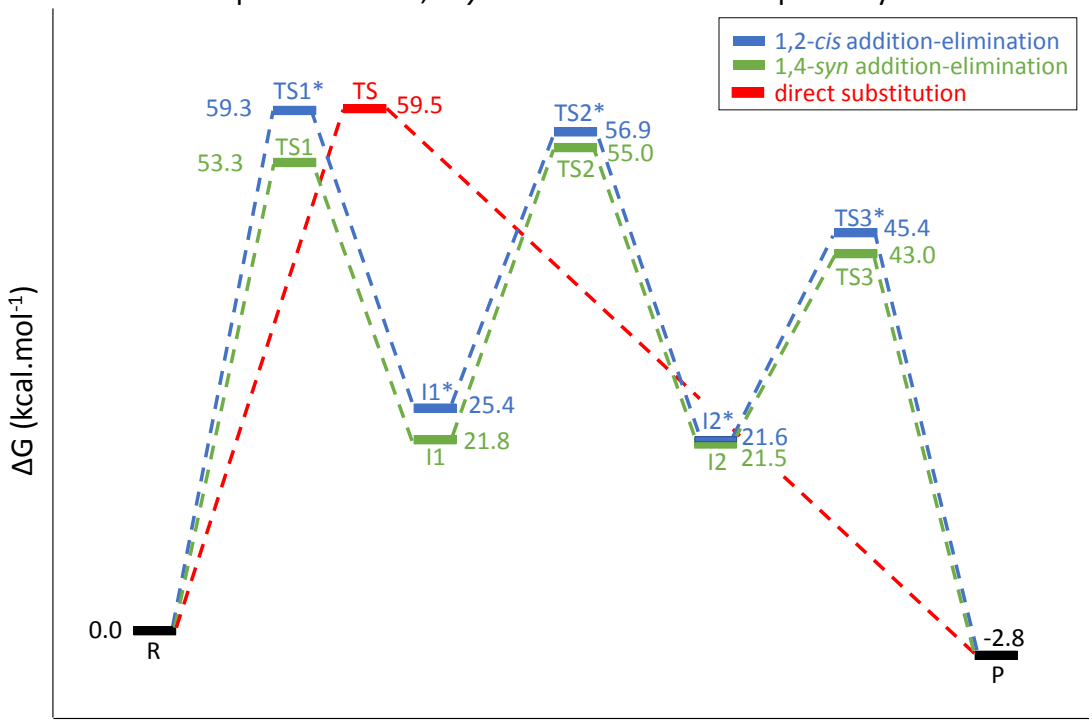

Figure 3. Gibbs free reaction profiles (in kcal.mol^{-1}) for the HBr assisted bromination of benzene in gas phase following a direct substitution (red), 1,2-*cis* (blue) or 1,4-*syn* (green) addition elimination pathway. The reactants (R) correspond to benzene, HBr and Br_2, while bromobenzene and 2 HBr molecules are obtained as products. The transition states are indicated with "*TS*", the intermediate states are labelled as "*I*".

Despite the more distinct kinetic preference for a 1,4-*syn* addition-elimination pathway as compared to the non-HBr assisted mechanisms, this finding can no longer be associated with a minimal disruption of the aromatic character of the rate-determining transition state. As such, Table 1 indicates that the HOMA index of the HBr-assisted 1,4-*syn* addition-elimination transition state (TS1) strongly decreased to a value of 0.579 (-0.321), while the remaining indices increased. This is a clear indication of a loss in aromatic behaviour. In contrast, the indices for the HBr-assisted 1,2-*cis* addition-elimination (TS1*) reactions remained more or less constant and based on both the bond length and bond order alternation it can even be

argued that this transition state is more aromatic as compared to the transition state of the 1,4-*syn* pathway. Moreover, the energetically least favourable transition state of the direct substitution pathway corresponds to the one where the aromaticity in the benzene ring is the least disturbed during the reaction, as evidenced by the highest HOMA index of 0.665 and the lowest aromatic fluctuation index. In order to explain the observed predilection for the 1,4-*syn* addition-elimination pathway, it is hence necessary to look beyond the changes in aromaticity. For this reason, the influence of non-covalent interactions was determined using the NCI index.[46] The two-dimensional plots comparing the attractive and repulsive interactions in the rate-determining transition state of the HBr-assisted 1,4-*syn* and 1,2-*cis* addition-elimination as well as the direct substitution pathways are shown in Figure 4. From these plots, no differences in the strength of the repulsive interactions between the reactants can be observed for the various pathways. In contrast, the attractive interactions in the rate-determining transition state of 1,4-*syn* addition-elimination are shifted to more negative values as compared to the 1,2-*cis* addition-elimination and direct substitution and are consequently stronger in nature. This explains the larger stability of this transition state and lower energetic barrier that needs to be overcome when the bromination occurs via the 1,4-*syn* addition-elimination pathway.

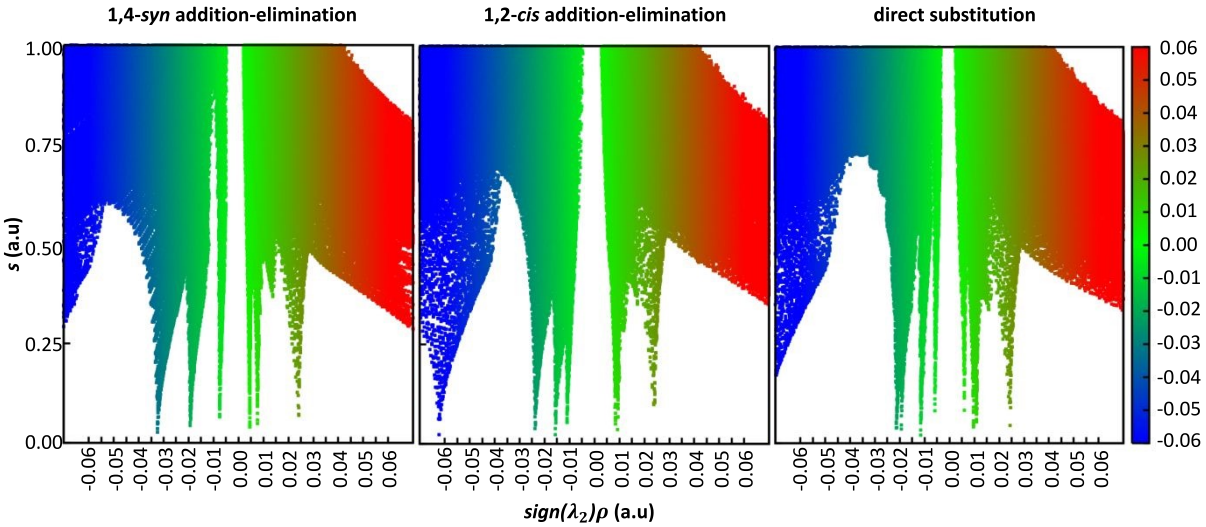

Figure 4. Non-covalent interaction analysis of the rate-determining transition state for the 1,4-*syn* (left) and 1,2-*cis* (middle) addition-elimination pathways as well as for the direct substitution (right) using two-dimensional plots of the reduced density gradient (*s*) versus the electron density multiplied by the sign of the second Hessian eigenvalue (λ_2). Attractive interactions are defined by negative values, while positive values represent repulsive interactions.

As most chemical reactions occur in the presence of solvent molecules, we subsequently establish the influence of apolar tetrachloromethane (CCl_4) and polar acetonitrile (ACN) on the reaction profiles of the HBr-assisted bromination using the implicit SMD model. Remarkably, throughout all calculations in both gas and solvent phase we never managed to retrieve a stable Wheland complex. In contrast, as can be observed from the Gibbs free reaction profiles for the bromination in CCl_4 (Figures S1 of the supporting information section) the previously assessed reaction paths remain valid in this reaction medium, though a decrease in activation energies for all transition states when compared to the HBr-assisted bromination in gas phase is retrieved. It is interesting to note that a non-polar solvent has a greater influence on the energetic barrier of the rate-determining step for the 1,2-*cis* addition-elimination (-7.0 kcal.mol^{-1}) and direct substitution (-7.1 kcal.mol^{-1}) reaction than for

View Article Online
DOI: 10.1039/D3CP03137C

the 1,4-*syn* addition elimination (-3.7 kcal.mol^{-1}). Nonetheless, with an activation energy of 49.7 kcal.mol^{-1} the 1,4-*syn* addition-elimination pathway remains the kinetically most favoured one in the presence of CCl_4. The favourable influence of solvation on the kinetic aspect of the different reaction paths is further accentuated in the polar acetonitrile (Figure S2 in the supporting information), especially for the 1,2-*cis* addition-elimination and direct substitution pathways where the activation energy of the rate-determining step decreased with 22.8 kcal.mol^{-1} and 22.5 kcal.mol^{-1}, respectively. In the case of the 1,4-*syn* addition-elimination reaction, transition state TS1 appears to be "only" lowered by 17.3 kcal.mol^{-1} compared to the gas phase situation. This observation can be ascribed to the difference in polarizability between each of the rate-determining transition states. In this regard, both the 1,2-*cis* addition-elimination and direct substitution are characterised by a rather similar polarizability α of 171.49 a.u. and 175.94 a.u., whereas for the 1,4-*syn* addition-elimination reaction a value of 160.25 a.u. is obtained. The lower polarizability of the latter can be attributed to the less pronounced NPA charge distribution between the benzene ring and the brominated reagents (Δq = 0.485 $|e|$), which hence makes the stabilising interactions with solvent molecules intrinsically less pronounced. In comparison, a charge distribution of 0.551 $|e|$ and 0.592 $|e|$ for the 1,2-*cis* addition-elimination and direct substitution is, respectively, found. Similar conclusions can be drawn from alternative charge schemes. As a result, the difference between the lowest energetic barrier belonging to the 1,4-*syn* addition-elimination (36.0 kcal.mol^{-1}) and the highest barrier for the direct substitution (37.0 kcal.mol^{-1}) only amounts to 1.0 kcal.mol^{-1}.

How do electron donating substituents affect the bromination of benzenes?

It is to be noted that as a result of the poor reactivity of benzene, the computed reaction barriers for the above-mentioned bromination reaction remain even in solvent rather high to be experimentally feasible. The kinetics of such an electrophilic aromatic halogenation reaction is, however, known to be potentially alterable through the judicious introduction of substituents. Moreover, these moieties allow to discriminate between the various carbon atoms of the benzene ring and hence introduce the concept of regioselectivity. In this context, Galabov *et al*. computed the reaction barriers of different competing HCl-assisted pathways that might occur during the chlorination of anisole.[27] This indicated that a concerted direct chlorination pathway without formation of the classic Wheland complex could energetically compete with a 2,3- or 3,4-addition-elimination mechanism, though the barrier of the rate-determining step for this substitution appeared to be systematically higher in energy independently of the used exchange-correlation functional. In addition, this study revealed that the classic *ortho*/*para*-regioselectivity, imputable to the electron donating nature of the substituent, was retained even for the kinetically preferred addition-elimination pathways and was qualitatively corroborated with experimental data in apolar CCl_4. Despite the intriguing conclusions of Galabov *et al*., a more systematic study regarding other halogenations (*i.e*. bromination or iodination) of substituted benzenes has to the best of our knowledge not yet been performed. As such, we herein discuss the influence of both an electron donating methoxy-group (anisole) and electron withdrawing nitro-group (nitrobenzene) on the mechanistic aspects of the HBr-assisted bromination reaction by constructing the Gibbs free energy profiles for a *(i)* direct substitution at *ortho, meta* or *para*, (*ii*) 3,4-addition-elimination at *meta* or *para,* (*iii*) 2,3- as well as (*iv*) 2,5-addition-elimination at *ortho* or *meta*. A schematical overview of these various pathways can be found in Figure 5.

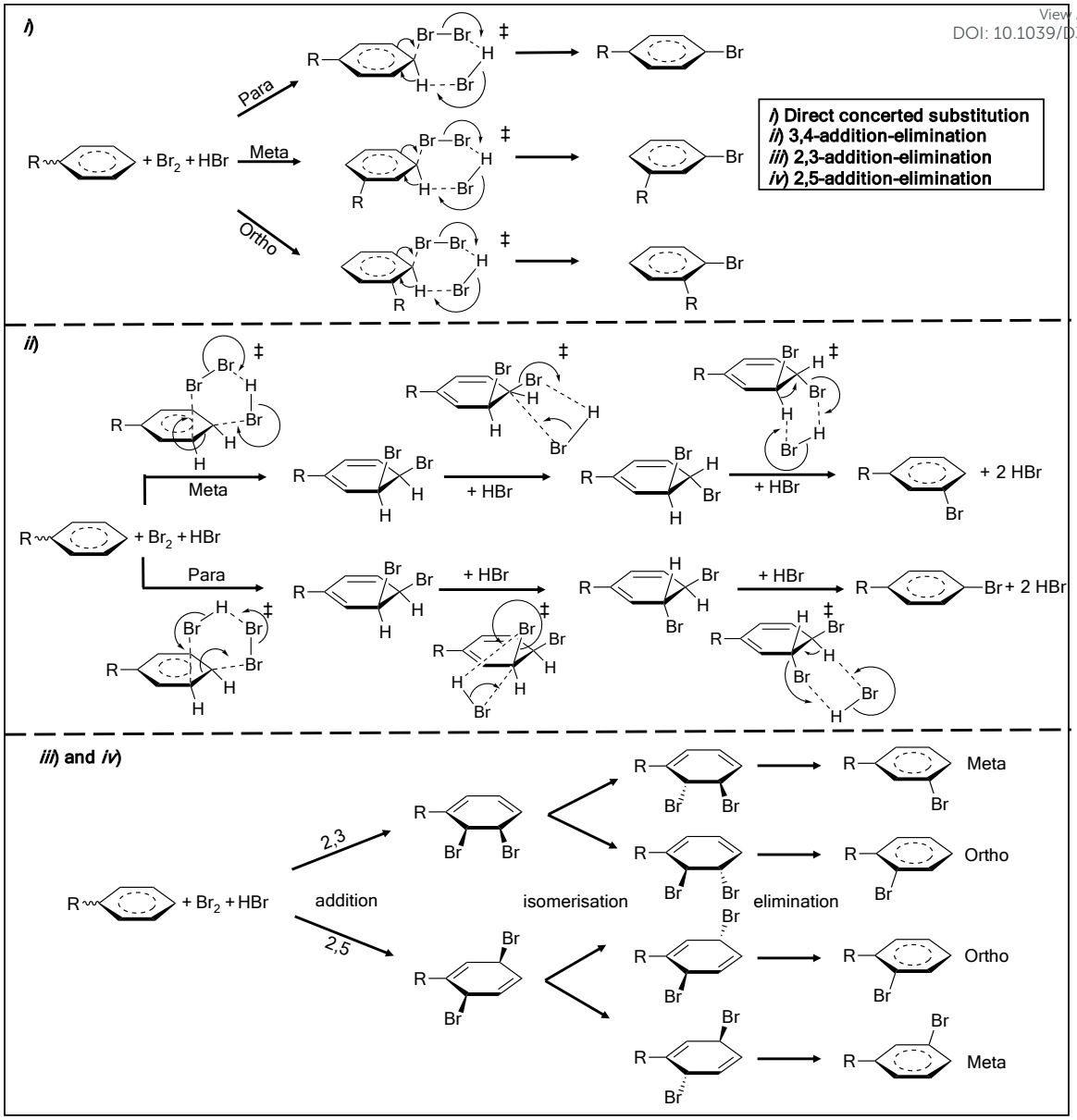

Figure 5. Overview of the various considered regioselective reaction pathways for the HBr-assisted electrophilic aromatic bromination of substituted benzenes. In this paper the substituent R corresponds to an electron donating methoxy (OMe) or electron withdrawing nitro (NO_2) moiety.

By analogy with the previous section, insight into the energetics of the various pathways is provided using geometrical (HOMA and BLA(1)) and electronic (FLU and BOA(1)) aromaticity indices in combination with the Wiberg bond indices and NCI index. The relative Gibbs free energies of the rate-determining transition states ($\Delta G^{\ddagger}$) with the corresponding aromaticity indices for the bromination of anisole can be found in Table 2, while the associated computed Gibbs free reaction profiles are shown in Figures S3-S6 of the Supporting Information. These profiles reveal that like chlorination,[27] the bromination of anisole via a substitution mechanism will proceed in a concerted manner with direct formation of the bromoanisole product and hence without prior generation of the Wheland intermediate, regardless of the regioselectivity of the attack. In line with the electron donating character of the OMe substituent, the preference for the *para*-substitution over the *ortho*-substitution (+1.6 kcal.mol^{-1}) is retrieved. The significantly higher activation energy of the concerted direct bromination at the *meta* position (61.8 kcal.mol^{-1}) also imply a rather low probability of

View Article Online
DOI: 10.1039/D3CP03137C

obtaining the *m*-bromoanisole product. This trend can nicely be traced back using the Fukui functions for electrophilic attack (f^-) condensed on the carbon atoms of the ring in anisole. The *para* position appears to be the most prone to donate its electrons given the highest f^- value of 0.223 a.u., while the condensed Fukui function for the *meta* carbon atoms drops to 0.033 a.u.. Accordingly, the kinetics of the anisole bromination reaction seems to be triggered by the intrinsic reactivity of the reactant. From the calculated aromaticity indices in Table 2 it can be noted that, unlike the bromination of benzene, a stronger transient perturbation in the aromatic behaviour of the ring system induces a decrease in the barrier height of the rate-determining step. In this regard, the HOMA index for the least favourable *meta*-substitution reaches a maximum value of 0.694, but drastically reduces to 0.398 when the attack at the *para* position is considered. The more pronounced aromatic character of the former transition state is also confirmed by the lowest values for the bond length alternation, bond order alternation as well as aromatic fluctuation index.

Table 2. Relative Gibbs free energies (ΔG‡, in kcal.mol^{-1}), structural and electronic aromaticity indices as well as Wiberg C-O bond index (WBI) and C-O bond distance (BD in Å) for the rate-determining transition state (TS1) of the HBr-assisted bromination of anisole in gas phase determined at the ωB97X-D/cc-pVTZ level of theory.

Mechanism	ΔG‡	HOMA	BLA(1)	BOA(1)	FLU	WBI[a]	BD[b]
Direct *ortho*-substitution	49.7	0.449	0.050	0.245	0.031	1.21	1.29
Direct *meta*-substitution	61.8	0.694	0.037	0.145	0.019	1.04	1.34
Direct *para*-substitution	48.1	0.398	0.059	0.296	0.034	1.18	1.30
2,3-*ortho* add-elim	51.3	0.298	0.047	0.193	0.031	1.16	1.30
2,3-*meta* add-elim	61.2	0.572	0.041	0.153	0.021	1.04	1.33
2,5-*ortho* add-elim	46.1	0.298	0.060	0.275	0.035	1.16	1.31
2,5-*meta* add-elim	53.6	0.658	0.044	0.191	0.020	1.04	1.34
3,4-*meta* add-elim	59.0	0.536	0.047	0.203	0.023	1.04	1.34
3,4-*para* add-elim	40.9	0.319	0.064	0.321	0.039	1.21	1.29

[a]Wiberg C-O bond index in anisole equals 1.02. [b]C-O bond distance in anisole amounts to 1.35 Å.

This seemingly counterintuitive finding appears entirely attributable to the amenability of delocalising electrons from the methoxy-substituent towards the ring as validated by non-aromaticity related indices like the Wiberg bond indices and bond distance between C and O. This reveals that the changes in both the C-O bond distance as the corresponding bond index for the *meta*-addition transition state with respect to the anisole reactant are minimal and hence the effect of electron delocalisation on the Gibbs free energy of this transition state is expected to be obsolete. In contrast, for the pathways with lower kinetic barrier, the bond distance decreases by 0.05-0.06 Å, while the corresponding Wiberg index increases to 1.18 and 1.21 for attack at *para* and *ortho*, respectively. In other words, this indicates that the bond between carbon and oxygen exhibits a more pronounced double bond character. Consequently, for benzenes bearing an electron donating moiety, the kinetic control of an electrophilic aromatic bromination benefits more from the delocalisation of electrons than from the retention of aromatic character in the benzene ring.

Although the direct concerted substitution pathways retain the expected textbook selectivity, these mechanisms turn out not to be energetically preferable. Indeed, Table 2 indicates that the activation energy of the rate-determining transition state for the most favourable addition-elimination pathway is systematically lower than for a concerted mechanism. Accordingly, a synthetical route towards the *p*-bromoanisole product involving a 3,4-addition-

View Article Online
DOI: 10.1039/D3CP03137C

elimination pathway appears to be 7.2 kcal.mol^{-1} more beneficial as compared to the *para*-substitution. In this mechanism, the kinetics of the reaction is entirely determined by the transition state corresponding to the asymmetric addition step (TS1), in which the bromine atom derived from Br_2 will interact with the *para*-carbon atom ($d_{C\text{-}Br}$ = 2.00 Å) significantly faster than the assisting Br atom derived from HBr ($d_{C\text{-}Br}$ = 3.31 Å). The rate-determining transition states together with key distances of the forming bond(s) for both pathways resulting into the *para* product are shown in Figure 6. It is worth noting that the lower energy barrier of such a non-symmetrical 3,4-addition to anisole comes with a further decrease in the aromaticity of the benzene ring, as the HOMA index slightly reduces to 0.319 (-0.079) with respect to the direct substitution. The delocalisation of electrons is also found to be more pronounced as a slight increase in double bond character of the C-O bond is observed. Besides the influence of this substituent effect (*i.e*. electron delocalisation), comparing the two-dimensional NCI plots of the transition states of interest (Figure 7) allows us to assess a difference in the strength of the attractive interactions. As such, a shift with respect to the *para*-substitution towards more negative values and hence stronger attractive interactions can be observed for the 3,4-addition step. This finding is quantitatively confirmed through the comparison of the integrated NCI volumes for attractive interactions. In this regard, the 3,4-addition-elimination volume amounts to 70.398 a.u. while for the direct substitution pathway this volume decreases to only 62.388 a.u.. As the difference in repulsive interaction strength between both pathways is significantly smaller (ΔV_{NCI} = 0.527 a.u.), we argue that the kinetic favourability of the 3,4-addition-elimination leading to *p*-bromoanisole is a direct consequence of both stronger electron delocalisation effects and attractive interactions.

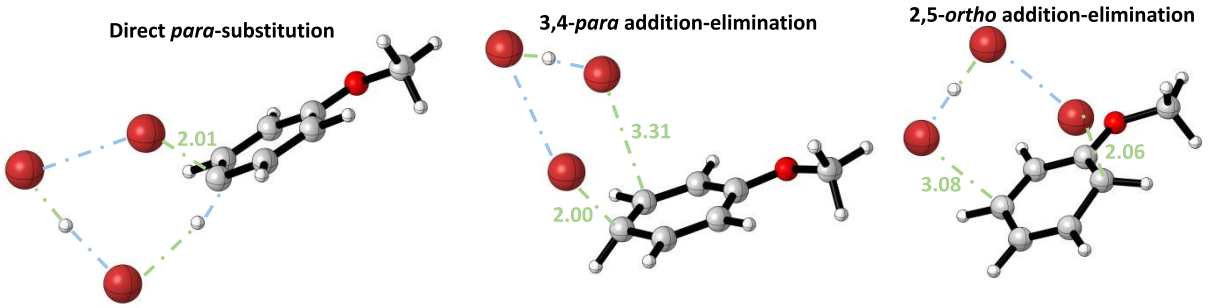

ΔG‡ = 48.1 kcal.mol^{-1}
BOA(1) = 0.296
WBI = 1.18

ΔG‡ = 40.9 kcal.mol^{-1}
BOA(1) = 0.321
WBI = 1.21

ΔG‡ = 46.1 kcal.mol^{-1}
BOA(1) = 0.275
WBI = 1.16

Figure 6. Rate-determining transition states with key distances (in Å) of the forming bond(s) for the direct *para*-substitution, 3,4-*para* and 2,5-*ortho* addition-elimination pathway.

A synergy between the aforementioned effects also appears to be the main reason why a bromination of anisole at *para* is energetically more advantageous than a reaction at the *ortho* position. Aside from the direct concerted substitution, the *o*-bromoanisole can be obtained from two competing addition-elimination pathways in which either a 2,3- or 2,5-intermediate product is being formed. With a reaction barrier of 46.1 kcal.mol^{-1} the 2,5-addition-elimination pathway appears to be 3.6 kcal.mol^{-1} and 5.2 kcal.mol^{-1} more favourable as compared to the concerted substitution and 2,3-addition-elimination pathway, respectively. As retrieved from Table 2, this rate-determining 2,5-addition transition state is characterised by lower values for the bond length alternation, bond order alternation and aromatic fluctuation index when compared to the 3,4-addition transition state. Hence, adding a bromine atom at the *ortho* position allows the benzene ring system to retain more aromatic character as compared to *para*-addition, but at the expense of a larger activation energy. It is

View Article Online
DOI: 10.1039/D3CP03137C

striking that HOMA is the only of the used aromaticity indices that does not support this observation. Nevertheless, as both the Wiberg bond index and the distance between the relevant carbon and oxygen atom confirm the enhanced partial double bond character of the 3,4-addition transition state, we put forward the importance of electron delocalisation in triggering *p*-bromoanisole over *o*-bromoanisole as major compound. Despite the close relationship between electron delocalisation and aromaticity, the divergent behaviour of the HOMA index in this particular case confirms the importance of determining, as described by Sola *et al.*,[53] the range of applicability for each of the used indices. Next, the integrated NCI volumes point out that both the attractive and repulsive interactions are more important in the 2,5-addition-elimination pathway, though the largest difference between *ortho*- and *para*-addition resides in the repulsive part. A three-dimensional representation of the non-covalent interactions in both transition states obtained for an isovalue of 0.5 (Supporting Information Figure S7) allow us to retrace the stronger repulsive interactions during the 2,5-addition to the presence of a large isosurface between the methoxy-substituent and bromine atom. This is assigned to a steric clash induced by the proximity of both moieties when *ortho* regioselectivity is being considered.

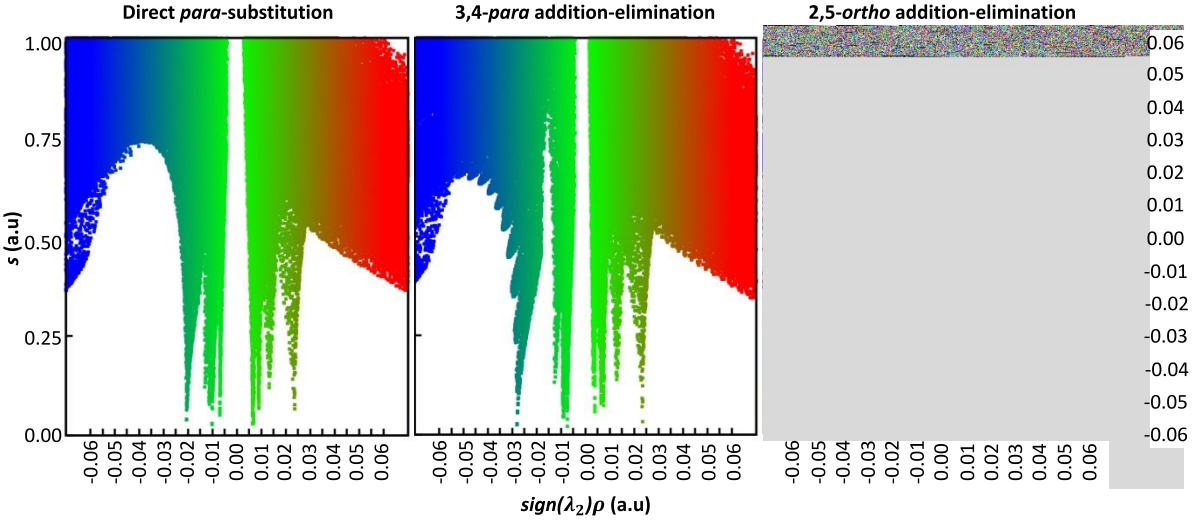

Figure 7. Non-covalent interaction analysis of the rate-determining transition state for the concerted *para*-substitution (left), 3,4-*para* (middle) and 2,5-*ortho* (right) addition-elimination pathways using two-dimensional plots of the reduced density gradient (*s*) versus the electron density multiplied by the sign of the second Hessian eigenvalue (λ_2). Attractive interactions are defined by negative values, while positive values represent repulsive interactions.

How do electron withdrawing substituents affect the bromination of benzenes?

Having assessed the influence of electron donation on the bromination reaction, we now shift to a prototypical example of a benzene ring with electron withdrawing group: nitrobenzene. The computed Gibbs free reaction profiles for the bromination of this compound are shown in Figures S8-S11 of the Supporting Information, while Table 3 lists the relative Gibbs free energies of the rate-determining transition states ($\Delta G^{\ddagger}$) together with the corresponding indices of interest. The transition state describing the bromination through a direct substitution pathway at the *ortho* position could only be found at the semi-empirical level of theory (PM6).[54] We therefore hypothesize the barrier for this particular reaction to be extremely high. The substitution pathways for the alternative *meta* and *para* products could be fully retrieved, but like previous compounds these turn out not to be kinetically favourable

View Article Online
DOI: 10.1039/D3CP03137C

approaches towards bromination of benzenes. The associated reaction barrier for *meta*-substitution reaches 68.7 kcal.mol^{-1} and is only 0.2 kcal.mol^{-1} more beneficial than the *para*-substitution. The high HOMA indices of 0.722 (*meta*) and 0.781 (*para*) furthermore reveal that the aromaticity of the benzene ring is only moderately affected and hence the substitution still proceeds via a single concerted transition state without formation of the intermediate σ-complex. Overall, the bromination of nitrobenzene seems to preferentially occur through an addition-elimination reaction, though it is noted that the activation energy for each of these rate-determining transition states is significantly more important than for anisole. In this regard, the global softness of nitrobenzene was found to be 3.55 eV smaller as compared to anisole. This conceptual DFT reactivity index confirms the lower propensity of nitrobenzene to undergo charge transfer reactions like the electrophilic halogenation and reinforces the observed deactivating influence of electron withdrawing groups on the kinetics of both the substitution and the addition-elimination reaction.

Table 3. Relative Gibbs free energies ($\Delta G^{\ddagger}$, in kcal.mol^{-1}), structural and electronic aromaticity indices and Wiberg C-N bond index (WBI) and C-N bond distance (BD, in Å) for the rate-determining transition state (TS1) of the HBr-assisted bromination of nitrobenzene in gas phase determined at the ωB97X-D/cc-pVTZ level of theory.

Mechanism	$\Delta G^{\ddagger}$	HOMA	BLA(1)	BOA(1)	FLU	WBI[a]	BD[b]
Direct *ortho*-substitution	n.a.	n.a.	n.a.	n.a.	n.a.	n.a.	n.a.
Direct *meta*-substitution	68.7	0.722	0.035	0.147	0.016	0.90	1.48
Direct *para*-substitution	68.9	0.781	0.027	0.144	0.014	0.89	1.49
2,3-*ortho* add-elim	69.4	0.561	0.048	0.204	0.021	0.90	1.48
2,3-*meta* add-elim	68.8	0.526	0.043	0.156	0.020	0.90	1.48
2,5-*ortho* add-elim	61.3	0.630	0.049	0.219	0.020	0.90	1.47
2,5-*meta* add-elim	60.7	0.612	0.048	0.213	0.020	0.90	1.48
3,4-*meta* add-elim	67.2	0.545	0.043	0.174	0.020	0.90	1.47
3,4-*para* add-elim	68.6	0.573	0.041	0.182	0.020	0.89	1.48

[a]Wiberg C-N bond index in nitrobenzene equals 0.91. [b]C-N bond distance in nitrobenzene amounts to 1.47 Å.

The reaction profiles clearly indicate that the differences in activation energy between the various mechanisms on one hand, but more importantly within one and the same pathway are significantly smaller with respect to anisole, suggesting a less pronounced regioselective behaviour. In line with classic organic chemistry textbooks, *m*-bromonitrobenzene nevertheless always emerges as the most favourable product from a kinetic point of view, followed by *ortho* and *para* in that order. Overall, the 2,5-addition-elimination mechanism appears to be the energetically most advantageous path to brominate nitrobenzene, as both approaches (*meta* (60.7 kcal.mol^{-1}) and *ortho* (61.3 kcal.mol^{-1})) are characterized by the lowest activation energy. On the other hand, the Fukui functions for electrophilic attack (f^-) condensed on the carbon atoms of the ring in nitrobenzene do not support these findings at all. With a f^- value of 0.091 a.u., the *para* position initially emerges to be substantially more reactive towards an electrophile than the *ortho* and *meta* carbon atoms for which the condensed Fukui functions amount to 0.030 a.u. and 0.025 a.u., respectively. Given the completely inversed trend between the kinetics of the reaction and the original local reactivity, it can be concluded that the halogenation of benzenes bearing an electron-withdrawing group is not affected by the intrinsic reactivity properties of the reactant. This observation is in line with previous energy decomposition analysis of *meta*-directing substituents performed by some of the authors.[55] Herein, it was shown that the preferred

View Article Online
DOI: 10.1039/D3CP03137C

meta selectivity could not be related to orbital interactions, as the strongest interaction between the reactant and electrophile was found for the *para* position.

According to Table 3, both the Wiberg index and distance of the C-N bond in the rate-determining transition states remain constant with respect to nitrobenzene, independently of the followed mechanism. The C-N bond index varies between 0.89 and 0.90, while the distance oscillates between 1.47 and 1.49 Å. The latter is in very close agreement with the sum of the covalent radii of a nitrogen and a sp^3 hybridised carbon atom,[56] quite surprisingly implying the almost preservation of pure single bond character during the key step of the bromination. Therefore, delocalisation of electrons from the ring towards the nitro moiety does not influence the energetic barrier of the rate-determining step. Moreover, the used aromaticity indices do not provide a unified picture of the exact impact of aromaticity distortion on the height of the reaction barriers. In this regard, it might at first sight be argued from the structural HOMA index that preservation of the benzene's aromaticity feature has an adverse effect on the activation energy of the addition reaction, as the largest HOMA values are systematically retrieved for the least favourable regioselective approaches. This perception is refuted by both the bond length alternation, which, like HOMA, belongs to the structural aromaticity indices, as well as by the bond order alternation. With the exception of the BLA(1) index for the 3,4-pathway, these indices suggest that the benzene ring in the energetically lower *meta* transition state exhibits more aromatic behaviour as compared to *ortho* or *para*. Given the quantitative small differences between the indices of the various regioselective approaches, we believe that unlike anisole, the extent to which the aromaticity is disturbed does not play a crucial role in the preference for the *meta* pathways. Additionally, the two-dimensional NCI plots in Figure 8 do not reveal significant differences in the attractive nor repulsive interactions between the 2,5-*ortho*- and *meta*-addition or 3,4-*para*- and *meta*-addition. Hence, regioselective preferences cannot be ascribed to these interactions neither. Conversely, these plots allow the rationalisation of the lower activation energy of a 2,5-addition elimination pathway compared to the 3,4-addition elimination pathway in terms of attractive interactions. Indeed, the 2,5-*meta*-addition is described by a larger number of attractive signals with enhanced strength as compared to the alternative 3,4-*meta*-addition.

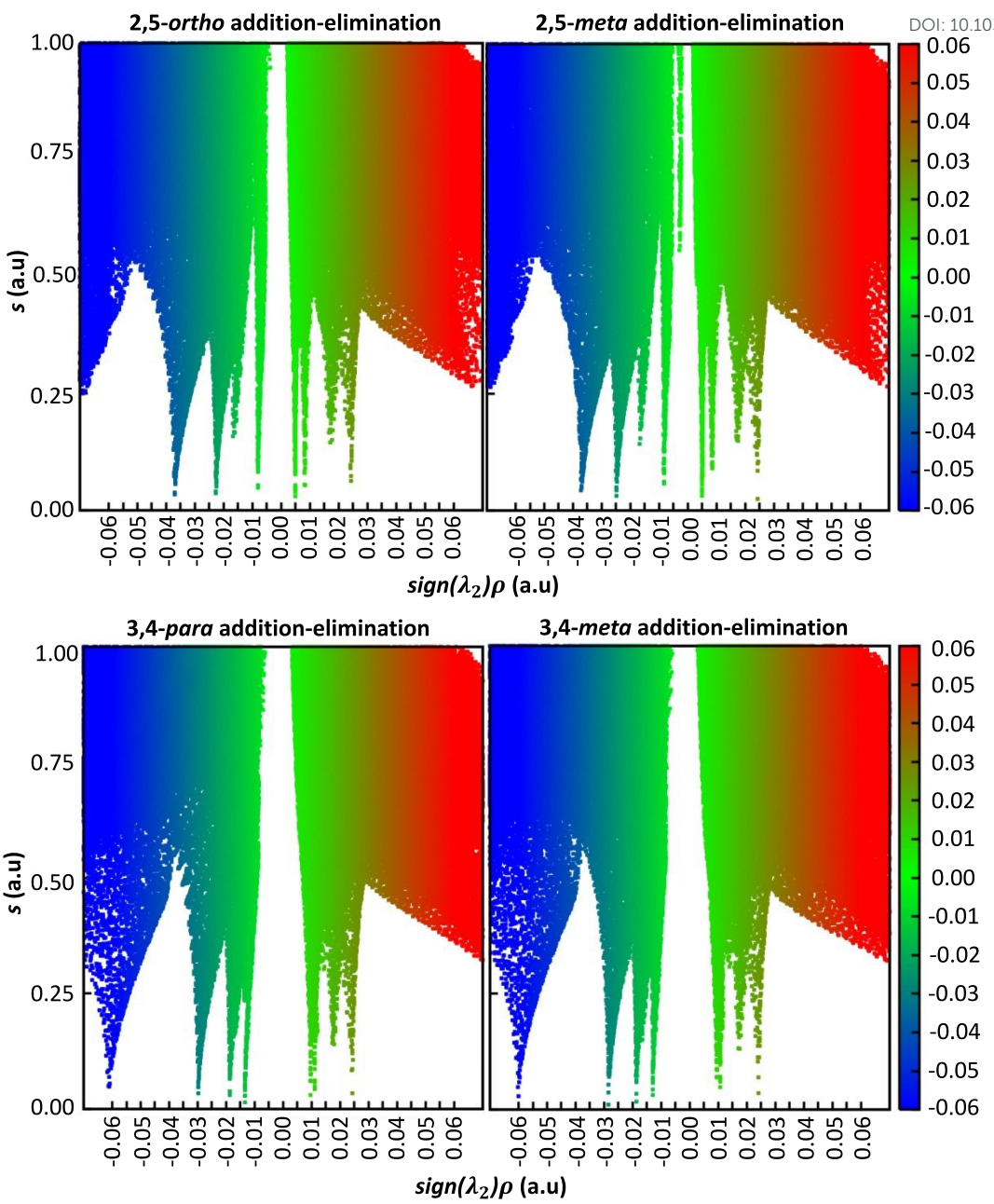

Figure 8. Non-covalent interaction analysis of the rate-determining transition state for the 2,5-addition-elimination (top) and 3,4-addition-elimination (bottom) pathways using two-dimensional plots of the reduced density gradient (*s*) versus the electron density multiplied by the sign of the second Hessian eigenvalue (λ_2). Attractive interactions are defined by negative values, while positive values represent repulsive interactions.

In other words, none of the parameters that were found to drive the regioselectivity of the bromination of anisole seem to apply for nitrobenzene. These observations together with the inversed trend between the activation energy of the rate-determining step and the reactivity indices of the nitrobenzene reactant enables us to assert that the bromination of this compound proceeds via transition states that are occurring later on the potential energy surface than those for anisole. This hypothesis is confirmed through computation of the root-mean-square deviation for the bond distances in both the addition transition state and subsequent reaction intermediate, which can be found in Table S2 of the Supporting Information. For each of the addition-elimination pathways, this deviation is systematically smaller for the bromination of nitrobenzene, hence these rate-determining transition states

View Article Online
DOI: 10.1039/D3CP03137C

exhibit more features of the intermediate addition product. The later nature of electrophilic aromatic substitution reactions on benzenes with *meta*-directing groups when compared to *ortho*/*para* directors was also previously proposed based on an energy decomposition analysis.[55] As a result, we expect the transition states to hold a partial positive charge inside the ring structure. This positive charge will be localised around the *ipso* carbon atom when a regioselective addition at the *ortho* or *para* position is considered, but not in the case of a bromination at *meta*. In this regard, the calculated NPA charge on the *ipso* carbon for the rate-determining 2,5-*meta*- or *ortho*-addition transition states amounts to -0.033 lel and 0.117 lel, respectively, whereas for the 3,4-addition-elimination pathway a charge of -0.033 lel (*meta*) and 0.166 lel (*para*) is obtained. Given the absence of electron delocalisation towards the substituent, which was proven by the constant C-N bond distance and Wiberg index, the nitrogen atom attached to the *ipso* carbon also carries a positive charge, independently of the regioselective approach. Consequently, we believe that the higher activation energies for pathways involving the *para* and *ortho* product are due to an electrostatic clash at the level of the *ipso* position, which disappears for the kinetically most favourable *meta* reaction path.

Conclusion

In this study we assessed the kinetically most favourable pathway for the bromination of benzene, anisole as well as nitrobenzene and determined the main factors affecting the regioselectivity of this reaction using a combination of indices at the ωB97X-D/cc-pVTZ level of theory. The computed energy profiles revealed a preference for an addition-elimination rather than substitution pathway, independently of the considered reactant. The commonly accepted Wheland intermediate was not identified in gas phase nor in dichloromethane or even the more polar acetonitrile. The introduction of a single HBr molecule was shown to have a beneficial effect on the activation energy of the bromination. Indeed, the reaction barrier of both the 1,4-*syn* and 1,2-*cis* addition-elimination bromination of benzene decreased with 6.6 kcal.mol^{-1} and 9.3 kcal.mol^{-1}, respectively, in the presence of the auto-catalytic HBr molecule. The clear preference for such an HBr-assisted 1,4-*syn* addition-elimination on benzene is triggered by the strength of the attractive interactions in the rate-determining transition state in the gas phase. Implicitly including solvent molecules appeared to have a larger favourable influence on the activation energies of the 1,2-*cis* addition-elimination and concerted substitution mechanism given the larger polarizability of their rate-determining transition states with respect to the 1,4-*syn* addition-elimination mechanism. For the sake of completeness, it should be mentioned that the explicit treatment of polar and/or protic solvents might potentially have a beneficial effect on the stability of ionic intermediates by establishing strong local interactions with the solute and hence affect the energetic favourability of a given reaction pathway. This effect is currently being investigated using *ab initio* metadynamics simulations and will be the subject of a subsequent publication.

In the case of anisole, the lowest reaction barrier for the rate-determining asymmetric addition of bromine was recovered for a 3,4-addition-elimination pathway (40.9 kcal.mol^{-1}) resulting in the *para* product. The two-dimensional NCI-plots allow the preference for the addition-elimination over direct *para*-substitution to be ascribed partly to stronger attractive interactions in the former mechanism. The higher barrier height of the *ortho*-2,5-addition-elimination (+5.2 kcal.mol^{-1}) is controlled by a steric clash induced by the proximity of the OMe-substituent and bromine atom, while the *m*-bromoanisole is expected to be obtained in

minor amounts due to the systematically larger activation energies. This regioselectivity is in full accordance with organic chemistry expectations and is attributed, on one side, to the intrinsic reactivity properties of the reactant as the calculated Fukui function for electrophilic attack (f^-) displays an identical trend as the activation energy ($f_p{}^- > f_o{}^- > f_m{}^-$). Additionally, both aromaticity indices and the Wiberg bond index reveal that the kinetic control of the electrophilic aromatic bromination of anisole benefits more from the delocalisation of electrons than from the retention of aromatic character in the benzene ring. In this context, the interaction between the *ipso*-carbon and oxygen atom of the methoxy-group shows more double bond character when bromination occurs at the *para* position, but at the expense of more distorted aromaticity.

The introduction of the electron-withdrawing nitro-substituent on the benzene ring completely changes this perception. Not only does the activation energy for this bromination appear significantly higher than for anisole due to the lower global softness of nitrobenzene and therefore less pronounced propensity for charge transfer, but also the driving forces behind the *meta*-selectivity turn out to be different. Accordingly, it was observed that the Wiberg C-N bond index for the rate-determining transition states remain unaffected with respect to the reactant implying the absence of any electron delocalisation effect, whereas aromaticity indices seemed unable to provide a unified view on the impact of aromaticity distortion. The inversed trend between the condensed Fukui functions for electrophilic attack and barrier heights prove that intrinsic properties of nitrobenzene do not influence the kinetic control of the corresponding bromination reaction neither. In contrast, the later nature of the rate-determining addition on nitrobenzene, proven by root-mean-square deviations of the bond lengths, involves the presence of a partial positive charge localised on the *ipso*-carbon atom of the ring structure already at the level of the *ortho* and *para* transition state, but not for *meta.* As the nitrogen atom attached to the *ipso* carbon also carries a positive charge, it is concluded that an electrostatic clash at the level of the *ipso* position causes the higher activation energies for *para* and *ortho* pathways. With this study we provide the field with thorough fundamental insights into the archetypical electrophilic aromatic bromination and summarized the main take home messages in Figure 9.

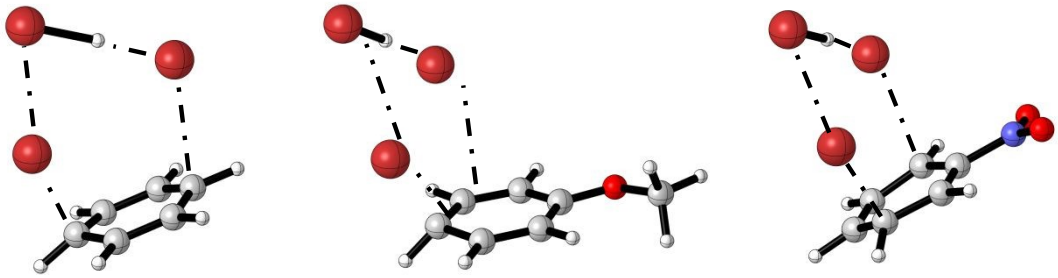

R = H

1,4-addition-elimination
$\Delta G^{\ddagger}$ = 53.3 kcal.mol^{-1}

Regioselectivity = none

R = CH_3 = EDG

3,4-addition-elimination
$\Delta G^{\ddagger}$ = 40.9 kcal.mol^{-1}

Regioselectivity = *para*

Intrinsic reactivity properties
Strongest electron delocalisation
Weakest repulsive interactions

R = NO_2 = EWG

2,5-addition-elimination
$\Delta G^{\ddagger}$ = 60.7 kcal.mol^{-1}

Regioselectivity = *meta*

Later nature of TS
Electrostatic clash at *ipso* carbon

Figure 9. General overview of the preferred bromination reaction mechanism and the driving forces behind the regioselectivity for each of the considered benzenes in this study.

View Article Online
DOI: 10.1039/D3CP03137C

Conflict of interest

There are no conflicts to declare.

Author contributions

Xavier Deraet: Investigation, Writing – original draft, Writing – review & editing
Eline Desmedt: Investigation, Writing – original draft, Writing – review & editing
Ruben Van Lommel: Investigation, Writing – original draft, Writing – review & editing
Veronique Van Speybroeck: Funding acquisition, Writing – review & editing
Frank De Proft: Conceptualization, Funding acquisition, Supervision, Writing – review & editing
Furthermore, all authors analyzed and discussed the results.

Acknowledgement

The authors gratefully acknowledge the Research Foundation-Flanders for the financial support through a research grant (G024019N). FDP also wishes to thank the Vrije Universiteit Brussel (VUB) for the support to his research group through a strategic research program. XD wishes to thank Jochen Eeckhoudt for the very fruitful brainstorming discussions. VVS acknowledges funding from the Research Board of the Ghent University. All computational resources and services used in this work were provided by the VSC (Flemish Supercomputer Center), funded by the Research Foundation - Flanders (FWO) and the Flemish Government. The graphical representations of the geometries were obtained using the freely available CYLview software.[57]

References

[1] D.G. Brown and J. Boström, *J. Med. Chem.,* 2016, **59**, 4443–4458.
[2] M. Mąkosza, *Chem. Eur. J.*, 2020, **26**, 15346–15353.
[3] A. Faust, *Ber. Dtsch. Chem. Ges.*, 1873, **6**, 1022–1023.
[4] W. J. Russell, *Proc. Chem. Soc.,* 1890, **6**, 95–106.
[5] S.D. Ross, *Prog. Phys. Org. Chem.*, 1963, **1**, 31–74.
[6] G.A. Olah, *Acc. Chem. Res.*, 1971, **4**, 240–248.
[7] J. Clayden, N. Greeves and S. Warren, *Organic Chemistry*, Oxford University Press, New York, 2012, 1512 p.
[8] M.G. Moloney, *Structure and Reactivity in Organic Chemistry*, Wiley-Blackwell, New Jersey, 2008, 320 p.
[9] S. Rohrbach, A.J. Smith, J.H. Pang, D.L. Poole, T. Tuttle, S. Chiba and J.A. Murphy, *Angew. Chem. Int. Ed.*, 2019, **58**, 16368–16388.
[10] I. Fernández, G. Frenking and E. Uggerud, *J. Org. Chem.*, 2010, **75**, 2971–2980.
[11] E.E. Kwan, Y. Zeng, H.A. Besser and E.N. Jacobsen, *Nat. Chem.*, 2018, **10**, 917–923.
[12] T. Stuyver and S. Shaik, *J. Am. Chem. Soc.*, 2021, **143**, 4367–4378.
[13] G. Koleva, B. Galabov, J. Kong, H.F. Schaefer III and P.v.R. Schleyer, *J. Am. Chem. Soc.*, 2011, **133**, 19094–19101.
[14] B. Galabov, D. Nalbantova, P.v.R. Schleyer and H.F. Schaefer III, *Acc. Chem. Res.*, 2016, **49**, 1191–1199.

[15] T. Stuyver, D. Danovich, F. De Proft and S. Shaik, *J. Am. Chem. Soc.*, 2019, **141**, 9719–9730.
[16] R. Van Lommel, S.L.C. Moors and F. De Proft, *Chem. Eur. J.*, 2018, **24**, 7044–7050.
[17] S.L.C. Moors, X. Deraet, G. Van Assche, P. Geerlings and F. De Proft, *Chem. Sci.*, 2017, **8**, 680–688.
[18] S. Rohrbach, J.A. Murphy and T. Tuttle, *J. Am. Chem. Soc.*, 2020, **142**, 14871–14876.
[19] N. Stamenković, N.P. Ulrih and J. Cerkovnik, *Phys. Chem. Chem. Phys.*, 2021, **23**, 5051–5068.
[20] Y. Nishii, M. Ikeda, Y. Hayashi, S. Kawauchi and M. Miura, *J. Am. Chem. Soc.*, 2020, **142**, 1621–1629.
[21] K. Smith and G.A. El-Hiti, *Green Chem.*, 2011, **13**, 1579–1608.
[22] D. Šakić and V. Vrček, *J. Phys. Chem. A*, 2012, **116**, 1298–1306.
[23] L.J. Andrews and R.M. Keefer, *J. Am. Chem. Soc.*, 1957, **79**, 5169–5174.
[24] A.V. Vasilyev, S.V. Lindeman and J.K. Kochi, *New J. Chem.*, 2002, **26**, 582–592.
[25] T. Delgado-Abad, J. Martínez-Ferrer, J. Reig-López, R. Mello, R. Acerete, G. Asensio and M.E. González-Núñez, *RSC Adv.*, 2014, **4**, 51016–51021.
[26] J. Kong, B. Galabov, G. Koleva, J.-J. Zou, H.F. Schaefer and P.v.R. Schleyer, *Angew. Chem. Int. Ed.,* 2011, **50**, 6809-6813.
[27] B. Galabov, G. Koleva, S. Simova, B. Hadjieva, H.F. Schaefer and P.v.R. Schleyer, *Proc. Natl. Acad. Sci. USA.,* 2014, **111**, 10067-10072.
[28] A.V. Shernyukov, A.M. Genaev, G.E. Salnikov, H.S. Rzepa and V.G. Shubin, *J. Comp. Chem.*, 2016, **37**, 210–225.
[29] M. Bocus, L. Vanduyfhuys, F. De Proft, B.M. Weckhuysen and V. Van Speybroeck, *J. Am. Chem. Soc. Au.*, 2022, **2**, 502–514.
[30] Gaussian 16, Revision A.03, M. J. Frisch, G. W. Trucks, H. B. Schlegel, G. E. Scuseria, M. A. Robb, J. R. Cheeseman, G. Scalmani, V. Barone, G. A. Petersson, H. Nakatsuji, X. Li, M. Caricato, A. V. Marenich, J. Bloino, B. G. Janesko, R. Gomperts, B. Mennucci, H. P. Hratchian, J. V. Ortiz, A. F. Izmaylov, J. L. Sonnenberg, D. Williams-Young, F. Ding, F. Lipparini, F. Egidi, J. Goings, B. Peng, A. Petrone, T. Henderson, D. Ranasinghe, V. G. Zakrzewski, J. Gao, N. Rega, G. Zheng, W. Liang, M. Hada, M. Ehara, K. Toyota, R. Fukuda, J. Hasegawa, M. Ishida, T. Nakajima, Y. Honda, O. Kitao, H. Nakai, T. Vreven, K. Throssell, J. A. Montgomery, Jr., J. E. Peralta, F. Ogliaro, M. J. Bearpark, J. J. Heyd, E. N. Brothers, K. N. Kudin, V. N. Staroverov, T. A. Keith, R. Kobayashi, J. Normand, K. Raghavachari, A. P. Rendell, J. C. Burant, S. S. Iyengar, J. Tomasi, M. Cossi, J. M. Millam, M. Klene, C. Adamo, R. Cammi, J. W. Ochterski, R. L. Martin, K. Morokuma, O. Farkas, J. B. Foresman, and D. J. Fox, Gaussian, Inc., Wallingford CT, 2016.
[31] J.D. Chai and M. Head-Gordon, *Phys. Chem. Chem. Phys.,* 2008, **10**, 6615-6620.
[32] T.H. Dunning, *J. Chem. Phys.,* 1989, **90**, 1007-1023.
[33] A.E. Reed, R.B. Weinstock and F. Weinhold, *J. Chem. Phys.*, 1985, **83**, 735-746.
[34] K.B. Wiberg, *Tetrahedron*, 1968, **24**, 1083-1096.
[35] NBO Version 3.1, E. D. Glendening, A. E. Reed, J. E. Carpenter and F. Weinhold.
[36] A.V. Marenich, C.J. Cramer and D.G. Truhlar, *J. Phys. Chem. B,* 2009, **113**, 6378-6396.
[37] R.G. Parr and R.G. Pearson, *J. Am. Chem. Soc.,* 1983, **105**, 7512-7516.
[38] K. Fukui, *Science,* 1982, **218**, 747-754.
[39] R.G. Parr and W.T. Yang, *J. Am. Chem. Soc.,* 1984, **106**, 4049-4050.
[40] W.T. Yang and W.J. Mortier, *J. Am. Chem. Soc.,* 1986, **108**, 5708-5711.
[41] J. Kruszewski and T.M. Krygowski, *Tetrahedron Lett.,* 1972, **13**, 3839-3842.

[42] I. Casademont-Reig, E. Ramos-Cordoba, M. Torrent-Sucarrat and E. Matito, *Molecules*, 2020, **25**, 711.
[43] a) E. Matito, M. Duran and M. Solà, *J. Chem. Phys.*, 2005, **122**, 014109; b) E. Matito, M. Duran and M. Solà, *J. Chem. Phys.,* 2006, **125**, 059901.
[44] E. Matito, ESI-3D: Electron Sharing Indices Program for 3D Molecular Partitioning; Institute of Computational Chemistry and Catalysis (IQCC), University of Girona, Catalonia, Spain, 2006; http://iqcc.udg.edu/~eduard/ESI/
[45] A.K. Todd, AIMAll (Version 19.10.12), TK Gristmill Software, Overland Park KS, USA, 2019 (aim.tkgristmill.com)
[46] E.R. Johnson, S. Keinan, P. Mori-Sanchez, J. Contreras-Garcia, A.J. Cohen and W. Yang, *J. Am. Chem. Soc.,* 2010, **132**, 6498-6506.
[47] J. Contreras-Garcia, E.R. Johnson, S. Keinan, R. Chaudret, J.-P. Piquemal, D.N. Beratan and W. Yang, *J. Chem. Theory Comput.,* 2011, **7**, 625-632.
[48] W. Humphrey, A. Dalke and K. Schulten, *J. Mol. Graph.,* 1996, **14**, 33-38.
[49] C. Riplinger and F. Neese, *J. Chem. Phys.,* 2013, **138**, 034106.
[50] C. Riplinger, B. Sandhoefer, A. Hansen and F. Neese, *J. Chem. Phys.,* 2013, **139**, 134101.
[51] F. Neese, *Wiley Interdiscip. Rev.: Comput. Mol. Sci.,* 2012, **2**, 73-78.
[52] F. Neese, *Wiley Interdiscip. Rev.: Comput. Mol. Sci.,* 2017, **8**, e1327.
[53] F. Feixas, E. Matito, J. Poater and M. Solà, *Chem. Soc. Rev.,* 2015, **44**, 6434-6451.
[54] J. J. P. Stewart, *J. Mol. Model.*, 2007, **13**, 1173-213.
[55] T. Fievez, B. Pinter, P. Geerlings, F.M. Bickelhaupt and F. De Proft, *Chem. Eur. J.*, 2011, **16**, 2958-2968.
[56] B. Cordero, V. Gomez, A.E. Platero-Prats, M. Reves, J. Echeverria, E. Cremades, F. Barragan, S. Alvarez, *Dalton Trans.,* 2008, **21**, 2832-2838.
[57] C.Y. Legault, CYLview, 1.0 b, Université de Sherbrooke, Canada, 2009; https://www.cylview.org/